Capacity Analysis Based on Channel Measurements of Massive MU-MIMO System at 3.5 GHz

Jie Xi[1], Jianhua Zhang[1,2], Senior IEEE Member, Lei Tian[1,2], Ye Wu[3]
[1]Key Lab of Universal Wireless Communications, Ministry of Education,
[2]State Key Lab of Networking and Switching Technology,
Beijing University of Posts and Telecommunications, Mailbox NO.92, Beijing 100876, China
[3]Huawei Technologies Co., Ltd.
e-mail: {xijie, jhzhang, tianlbupt}@bupt.edu.cn

***Abstract*—Massive multiple-input multiple-output (MIMO) is considered as one of the promising fifth Generation (5G) technologies, one of its key properties is the favorable propagation condition which describes mutual orthogonality among channels to different users. In this paper, we investigate to what extent the favorable condition can be realized by increasing the number of transmitting antennas (Tx) to 256 in a practical Urban Macro (UMa) scenario based on channel measurements at 3.5 GHz. Multi-user MIMO (MU-MIMO) capacity based on the zero forcing block diagonalized (ZFBD) scheme is evaluated, and the results are compared to the independent identically distributed (i.i.d.) channel. The performance improvements are found to decelerate at 64 Tx and certain gap from i.i.d. channel remains for all cases. The eigenvalue distributions of the composed two users' channel matrix are then checked, and very limited decorrelation of the users' sub-channels is observed. Finally, we consider number growths of receiving antennas (Rx) and numerical results indicate that the capacity gain is dependent on the scenario conditions and the antenna configurations at both Rx and Tx sides, although sustained growths are observed. Therefore, the full gain of favorable propagation is not entirely achieved in our measured practical channel environment.**

Keywords-massive MIMO; channel measurement; MU-MIMO; capacity; eigenvalue

I. INTRODUCTION

Facing the ever-increasing traffic demand stimulated by the explosive growth of smart devices and mobile Internet, three-dimensional (3D) MIMO with massive antennas at the transmitter and/or receiver side is envisioned as one of the promising key technologies for 5G era [1]. The performance gain in real-world field measurements of 3D fading channel model including the elevation angle [2] has been studied and reported in [3], [4]. The concept of massive MIMO is first introduced by T. L. Marzetta from Bell Laboratories in 2010 [5]. Massive MIMO can offer remarkably improved spatial resolution and greater degrees of freedom, and enhance the advantages of MU-MIMO systems by neglecting the effect of small-fading [6] and providing asymptotically favorable propagation between user channels [7]. However, users may be close to each other and share common scatterers in practical mobile communication systems, so that the level of realization of "favorable propagation" condition in practical environment maintains a concerning topic. There have already existed some measurement campaigns considering massive MU-MIMO performance in current literatures. In [8], [9], researchers from Lund University have considered a residential area at 2.6 GHz with a bandwidth of 50 MHz and studied singular value spreads and the sum-rate capacities with both linear and optimal precoding schemes, two types of 128-element array (virtual linear array and cylindrical array) are used and with one-element users. The results indicate that the user channels can be decorrelated by using reasonably large antenna arrays. Carrier frequency of 5.8 GHz with 100 MHz is also studied by Aalborg University [10], [11]. Performances of eigenvalues indicating inter- and intra- user properties are investigated for the impact of antenna aperture across different frequencies with three types of 64 antennas and eight 2-antenna users. Conclusions are drawn that larger aperture performs closer to the performance of i.i.d. channel and achieves more stable channel properties across different frequencies.

In consideration of looking into a larger number range of antennas at both Tx and user sides, our group conduct a series of virtual massive MU-MIMO channel measurements at 3.5 GHz for a bandwidth of 200 MHz. The rationality of the virtual measurement is proved in [12], with parameters including the power delay profile (PDP) and spatial angular characteristics calculated from combined channel impulse responses (CIRs) fitting well with the results directly collected from the measurement campaigns. In this paper, we compare the measured MU-MIMO channel capacity results for two 2-antenna users as the number of Tx increases to 256 with the i.i.d. channel. Normalized eigenvalue distribution is then investigated to get a visual view of the overall orthogonality performance of the users' sub-channels. The capacity gaps are also studied by increasing the number of antennas selected from the OmniDirectional Array (ODA) equipped for each user from 2 to 16, with 32 and 256 antennas equipped at Tx side, respectively.

The rest of the paper is organized as follows. In Sec.II, measurement system and scenario are introduced. Sec.III contain the data processing of the CIRs and the performance evaluation scheme. Numeric results and analysis are given in Sec.IV, and conclusions are drawn in Sec.V.

978-1-5090-6351-2/17/$31.00 ©2017 IEEE

1/5	2/6	3/7	4/8
9/13	10/14	11/15	12/16
17/21	18/22	19/23	20/24
25/29	26/30	27/31	28/32

(a) Photo and sketch of UPA

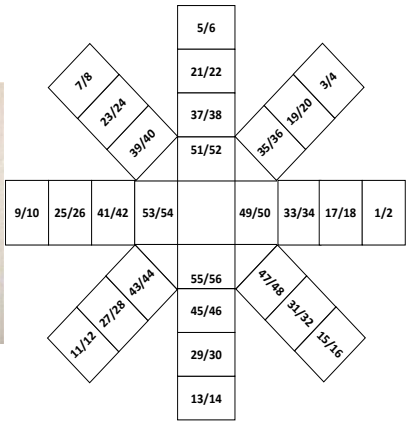

(b) Photo and sketch of ODA

Figure 1. Antenna arrays of Tx and Rx.

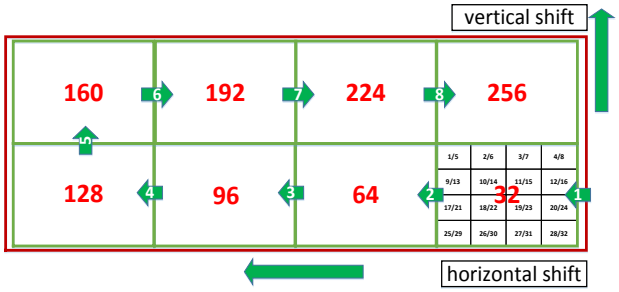

Figure 2. Illustrtion of the virtual 256-element UPA at Tx side.

II. CHANNEL MEASUREMENTS

A. Measurement System

The channel information is captured by the Elektrobit Prop-Sound channel sounder [3], at the carrier frequency of 3.5 GHz, with an effective bandwidth of 200 MHz. Periodic pseudo random binary sequence (PN) is chosen as the transmitting signal for the sounder which works in a time-division multiplexing mode. A high speed antenna switching unit is used at each of the transceiver side to sound all the antenna pairs in one sampling cycle (snapshots). The synchronization between the transmitting antennas and receiving antennas is realized by rubidium clock.

The antenna arrays used at Tx and Rx sides are shown in Fig.1. In the field measurement, as shown in [12], a 32-element Uniformed Panel Array (UPA) is used to form a vitual 256-element antenna array at the Tx side, by shifting the position for eight times as shown in Fig.2. At the two users' side, 16 antenna elements from the 56-element ODA are selected for each user. The distance between the two fixed ODA is set to be 20λ, where λ represents the wavelength. The detailed configurations of the antennas and the sounder are shown in Table I.

TABLE I. ANTENNA AND SOUNDER CONFIGURATIONS OF THE MEASUREMENT

Parameter		Value	
Antenna type		ODA (Rx)	UPA (Tx)
Number of antenna ports		16 (8 dual polarized)	32 (16 dual polarized)
Cross polarization		$\pm 45^o$	$\pm 45^o$
Antenna interval		$\lambda / 2$	$\lambda / 2$
Distribution of antennas		cylinder	planar
Angle range	***Azimuth***	$-180^o \sim 180^o$	$-70^o \sim 70^o$
	Elevation	$-70^o \sim 90^o$	$-70^o \sim 70^o$
Bandwidth		200 MHz	
PN length		255 chips	
No. of cycles		500 / spot	
Carrier frequency		3.5 GHz	
Distance between 2 users		1.72 m (20λ)	

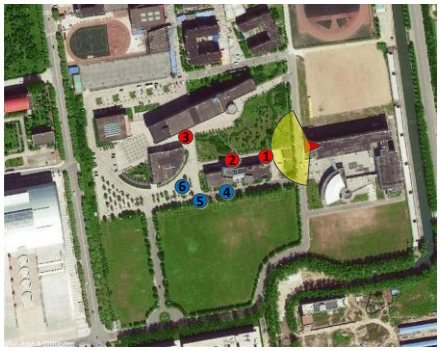

Figure 3. A overview of the measurement scenario. (The six dots are the positions selected for the Rx spots, and the red triangle indicates the Tx location with the yelow section denoting the angle range of the UPA.)

B. Measurement Scenario

The channel measurement campaign is carried out on the Hongfu Campus of Beijing University of Posts and Telecommunications (BUPT), China, a typical UMa scenario, as shown in Fig. 3. To ensure the stability of the measurement environment, occasions of less pedestrians and vehicles are carefully chosen during the measurements. Tx is mounted on the top of a 6-floored teaching building, which overlooks the surrounding buildings. Rx spots under LoS and NLoS conditions are selected and depicted as red and blue dots in Fig.3, respectively. Both of the Tx and Rx antennas are fixed and static in the measurements. The specific values of the measurement scenario are listed in Table II. Considering the virtual UPA has a much larger size than the ODA used in the measurements, the Rayleigh distance $R = \frac{2D^2}{\lambda}$ is calculated, where D is taken as the length of the UPA. As shown in

Table II, all the spots arranged in our measurements are in the far field region, thus the plane wave assumption can still be applied in our analyses.

TABLE II. DETAILED CONFIGURATIONS OF THE SCENARIO

Parameter	Value
Carrier frequency	3.5 GHz
Dimension of UPA (length × width)	0.68×0.34 m^2
Rayleigh distance	11.01 m
Height of Tx	26.2 m
Height of Rx	1.9 m
Rx spot	**Horizontal distance from Rx to Tx(m)**
Pos1	58
Pos2	97
Pos3	167
Pos4	101
Pos5	149
Pos6	172

III. DATA PROCESSING

The CIRs are derived from the raw datas obtained by the channel sounder. We consider a two-user massive MIMO downlink channel consisted of *M* Tx (elements) and *N* Rx (elements) for each user. By applying the Fast Fourier Transformation (FFT) to the time-delay domain CIR matrix, the *u*th user's channel is denoted as $\mathbf{H}_u^{CIR}(t, f) \in C^{N \times M}$, and a discrete sample of which can be written as

$$\begin{aligned} \mathbf{H}_u^{CIR}(j,k) &= \mathbf{H}_u^{CIR}(t, f)\big|_{t=j\cdot\Delta t,\, f=k\cdot\Delta f} \\ &= \mathbf{H}_u^{CIR}(j\cdot\Delta t, k\cdot\Delta f), \end{aligned} \tag{1}$$

where *j* and *k* represent the *j*th and *k*th sample bin in the time and frequency domain, respectively.

Normalization is then applied to the CIR channel matrix of each user to remove the effect of large scale fading between different spots and users, which is achieved as

$$\mathbf{H}_u(j,k) = \sqrt{\frac{N \times M}{\left\|\mathbf{H}_u^{CIR}(j,k)\right\|_F^2}}\mathbf{H}_u^{CIR}(j,k), \tag{2}$$

where $\|\cdot\|_F$ denotes the Frobenius norm. Thereby, the difference between different frequency/time bins and antenna pairs are kept for each user's channel matrix.

A. MU-MIMO Capacity

For the 200 MHz wideband channel, we calculate capacity on each frequency bin to meet the flat-fading demand. In this work, the number of users simultaneously served is considered as two, so the time-frequency CIR sample of each user is represented as $\mathbf{H}_u(j,k)|_{u=1,2}$. Assuming that the channel state information (CSI) is known at both Tx and Rx sides, then the statistical MU-MIMO sum capacity derived by ZFBD scheme realized in [13], [14] and our team's previous work [3] is given by

$$C_{MU} = \frac{1}{J}\frac{1}{K}\sum_{j=1}^{J}\sum_{k=1}^{K}\log_2\left(\mathbf{I} + \bar{\mathbf{\Lambda}}^2(j,k)\cdot\mathbf{\Sigma}\right), \tag{3}$$

where *J* and *K* is the total number of the time and frequency bins, $\mathbf{\Sigma}$ is the optimal power loading coefficient matrix, and $\bar{\mathbf{\Lambda}}$ is the block diagonalized matrix [3], [13], respectively.

B. Eigenvalue

By checking the properties of the eigenvalues of the correlation channel matrix, we can get a further intuitive view of the spatial streams' distribution condition as the number of Tx grows up. The composed two-user channel matrix is expressed as $\mathbf{H}(j,k) = \left[\mathbf{H}_1^T(j,k), \mathbf{H}_2^T(j,k)\right]^T$, then the statistical channel correlation matrix can be defined as

$$\mathbf{R} = E\{\mathbf{R}(j,k)\} = E\{\mathbf{H}(j,k)\mathbf{H}^H(j,k)\}. \tag{4}$$

By performing the singular value decomposition (SVD) operation to $\mathbf{R}$, the eigenvalues can be obtained as

$$Eigen\{\mathbf{R}\} = \{\lambda_i, i = 1,2,...,\min\{M,2N\}\}, \tag{5}$$

where $\min\{M,2N\}$ is the rank of the correlation matrix and the positive eigenvalues λ_i represent the power gains of streams [15]. We assume $\{\delta_i, i = 1,2,...,\min\{M,2N\}\}$ to represent the *i*th largest of the normalized eigenvalues $\left\{\lambda_i \Big/ \sum_{l=1}^{\min\{M,2N\}}\lambda_l\right\}$ in our analyses.

IV. RESULT ANALYSIS

For this section, we analyze the channel performance extracted from the practical virtual massive MIMO measurements for a typical UMa scenario at 3.5 GHz. The MU-MIMO capacity and the eigenvalue performances of the two 2-antenna users are considered for the increasing numbers of Tx. At last, the capacity results for different numbers of Rx elements are given for 32 Tx and 256 Tx.

A. MU-MIMO Capacity

Utilizing the closed-form sum capacity formula based on ZFBD scheme introduced in (3), the two-user MU-MIMO capacity results for the measurement channel and the ratio of that to i.i.d. channel are shown in Fig.4 and Fig.5, with *N* equal to 2 and *M* taking the value of 8, 16, 32, 64, 128 and 256, respectively. The 2 antennas selected from the ODA for each user are a pair of 2 dual-polarized antennas that receive the strongest signal strength (antenna No.1 and No.2 in Fig. 1(b)). While the antenna selection from the virtual UPA at Tx side is according to the port number and the shifting order of the UPA instructed in Fig. 1(a) and Fig. 2.

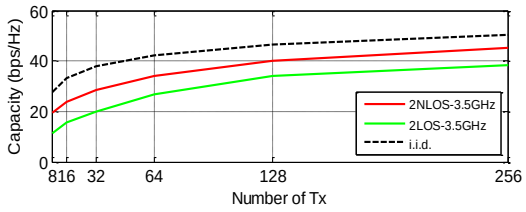

Figure 4. Capacity results for measured and simulated i.i.d. channel

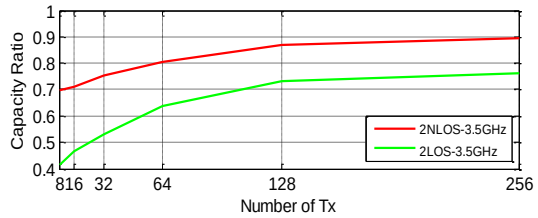

Figure 5. Capacity ratio of measured to simulated i.i.d. channel.

As shown in Fig. 4, we can see that the capacity for NLoS condition is larger than that for LoS condition. Since the campus we chosen as UMa scenario is in a suburb environment where scatterers are not so rich and the area is relatively open, the channel is mainly dominated by the LoS path for LoS condition, and the waves having better dispersions in NLoS condition achieve less correlated two users' sub-channels and thus better capacity performance. Considering the capacity performance in terms of ratio to i.i.d. channel as shown in Fig. 5, we can see that the measurement sum capacity ratio can reach 80% & 63% for NLoS & LoS conditions at 64 Tx, and 86% & 73% for NLoS & LoS conditions at 128 Tx, respectively. And the capacity ratio improvements for both conditions by continuing to increase *M* are less than 3%. Therefore, it is observed that the improvements of capacity ratio to i.i.d. channel achieved by increasing *M* slow down after it reaches 64 and gradually saturate at a certain value for all curves, that is, the "favorable condition" is not realized in our practical channel measurement environments.

B. *Eigenvalue*

To get a visual view of the orthogonality feature of the users' sub-channels, we derive the eigenvalues of the correlation matrix of the composed two-user channel by (5). As shown in the two figures in Fig. 6, each four-color bar is composed of the four normalized eigenvalues in a descending order and stacked from bottom to top. The size of each part in a bar represents the power of each streams, thus when the distribution gets more uniform, the users' sub-channels become less correlated, and a larger sum capacity is achieved. We can see that the results match up with the conclusions observed for the capacity performances in Sec.IV-A, where NLoS condition has more uniform eigenvalue distribution than LoS condition, in the form of the largest value getting smaller and the other three getting larger. It is also observed that, in our practical measurement environment, the state of equalization between the four streams is not achieved as *M* increases to 256. Hence there is still a certain gap existed to realize the orthogonal sub-channels of different users.

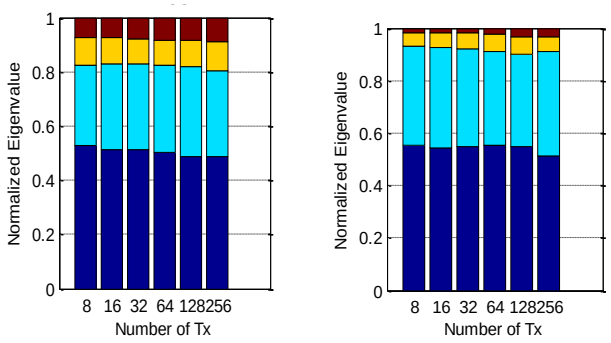

(a) 2NLoS-3.5GHz (b) 2LoS-3.5GHz

Figure 6. Normalized eigenvalue distribution of measured two 2-element users' channel matrix for different numbers of antennas at Tx side.

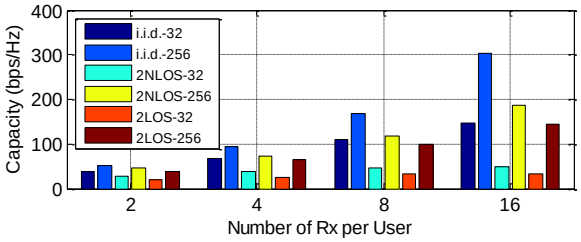

Figure 7. Capacity results for different numbers of antennas equipped at each user side.

C. *Varying Rx Antenna Numbers*

Fig. 7 shows the MU-MIMO capacity results for increasing the antenna numbers at the user side. For *M* chosen as 32 and 256, the receiving antennas for each user *N* is chosen as 2, 4, 8 and 16, respectively. The Rx antenna selection is from the bottom circle of ODA and according to the port number indicated in Fig. 1(b). The channel capacity is limited by the smaller number between the transmitting and receiving antennas, so that considerable capacity growths are obtained by increasing the numbers of Rx, as shown in Table III. However, as visually shown in Fig.7, the tendency to i.i.d. channel is not well achieved as *N* increases. One consideration is that the distance between the two users is fixed and relatively close, so that common scatterers may be shared by the users. On the other hand, we orientate antenna No.1 and No.2 of the ODA to the direction of Tx in the measurements, so that the signal waves received by the other 14 selected antennas are blocked to some extent from the Tx, considering the cylindrical shape of the ODA. Thus although the capacity gain can take advantage of the increasing antennas, user channels probably get more similar.

As shown in Table III, less capacity gaps are found for LoS condition on account of the dominant main path. And the gaps achieved are lowered down as *N* keeps increasing, which may be explained by the antenna sketch. As depicted in Fig. 1(b), the 4 antennas increased as *N* grows form 4 to 8 are at the back side (not facing the Tx) of the ODA, and *N*

growing from 8 to 16 means taking consideration of the other semi-circle side of the bottom antenna circle of the ODA, so that the gap values decreasing with a growth of *N* may due to the inferior positions of the added antennas. In addition, larger gaps are found for 256 Tx in all conditions, and the capacity gaps between *N* growing from 4 to 8 and 8 to 16 are closer than those for 32 Tx. The observations may be explained by the capability of 256 Tx to make use of a larger channel matrix, and for LoS condition, the antennas at the back side of the ODA actually behave as in NLoS condition, so that the UPA expanding to 256 Tx can make more use of the scatterers in the open UMa scenario. Over all, the MU-MIMO capacity of increasing the antennas at Rx side in our measurements is related to the antenna configurations at both the user and Tx sides, better performances are achieved by increasing the numbers of Tx to 256, however certain distance from i.i.d. channel still exists in our practical environment measurements.

TABLE III. CAPACITY GAP($\frac{C_{MU}(N=b)-C_{MU}(N=a)}{C_{MU}(N=a)}\times 100\%$)

Cases			***a*=2, *b*=4**	***a*=4, *b*=8**	***a*=8, *b*=16**
3.5 GHz	**NLoS**	**32Tx**	31.6%	24.3%	3.6%
		256Tx	62.6%	59.2%	59.0%
	LoS	**32Tx**	29.9%	22.6%	0.3%
		256Tx	69.0%	54.1%	45.0%

V. CONCLUSION

The two-user MU-MIMO capacity based on the ZFBD scheme and distribution of eigenvalues are discussed for increasing the numbers of Tx from 8 to 256, in a practical UMa scenario at 3.5 GHz. By comparing the performance to the i.i.d. channel, the ratios of above 63% and 73% are achieved for the number of Tx reaching 64 and 128, respectively, and little improvements are found when keeps increasing the numbers. And a really slight trend is observed to the uniform distribution of eigenvalues as the number of Tx grows up. Therefore, the more decorrelated user channels and more equalized sub-channels are achieved for massive MIMO than conventional MIMO, but the gaps to i.i.d. channel are still existed in our studied measurement environment. We also discuss the capacity results for increasing numbers of antennas equipped at each user, the performances are observed to be influenced by the antenna configurations at both Tx and Rx sides. So that the "favorable condition" indicating the orthogonal user channels is not realized in our measurement scenario. Since our work in this paper only assumes two fixed users both on the ground level, more users and users distributing on different floors are going to be considered in our future work.

ACKNOWLEDGMENT

The research is supported in part by National Science and Technology Major Project of the Ministry of Science and Technology (2017ZX03001012-003), National Natural Science Foundation of China (NO. 61322110), Doctoral Fund of Ministry of Education (20130005110001), and the Ministry of Education-China Mobile Research Fund (MCM20160105). Field measurements are funded by Huawei Technologies Co., Ltd.

REFERENCES

[1] Global TD-LTE Initiative (GTI), "Massive MIMO white paper V0.1," https://www.lte-tdd.org/news/gti/2017-03-01/10188.html, Mar. 2010.

[2] J. H. Zhang, C. Pan, F. Pei, G. Y. Liu, and X. Cheng, "Three-dimensional fading channel models: A survey of elevation angle research," *IEEE Communication Magazine*, vol. 52, no. 6, pp. 218–226, Jun. 2014.

[3] J. H. Zhang, Y. X. Zhang, Y. W. Yu, R. J. Xu, Q. F. Zheng, and P. Zhang, "3-D MIMO: how much does it meet our expectations observed from channel measurements?," *IEEE Journal on Selected Areas in Communications*, vol. 35, no. 8, pp. 1887-1903, Aug. 2017.

[4] X. Cheng, B. Yu, L. Q. Yang, J. H. Zhang, G. Y. Liu, Y. Wu, and L. Wan, "Communication in the real world: 3D MIMO," *IEEE Wireless* Communications, vol. 21, no. 4, pp. 136–144, Aug. 2014.

[5] T. L. Marzetta, "Noncooperative cellular wireless with unlimited numbers of base station antennas," *IEEE Transactions on Wireless Communications*, vol. 9, no. 11, pp. 3590-3600, Nov. 2010.

[6] F. Rusek, D. Persson, B. K. Lau, E. G. Larsson, T. L. Marzetta, O. Edfors, and F. Tufvesson, "Scaling up MIMO: opportunities and challenges with very large arrays," *IEEE Signal Processing Magazine*, vol. 30, no. 1, pp. 40-60, Sep. 2013.

[7] H. Ngo, E. Larsson, and T. Marzetta, "Aspects of favorable propagation in massive MIMO," in *2014 Proceedings of the 22nd European Signal Processing Conference (EUSIPCO)*. The European Association for Signal Processing, 2014, pp. 76-80.

[8] X. Gao, O. Edfors, F. Rusek, and F. Tufvesson, "Massive MIMO performance evaluation based on measured propagation data," *IEEE Transactions on Wireless Communications*, vol. 14, no. 7, pp. 3899-3911, Jul. 2015.

[9] X. Gao, O. Edfors, F. Rusek, and F. Tufvesson, "Linear pre-coding performance in measured very large MIMO channels," in *2011 74th IEEE Vehicular Technology Conference (VTC Fall)*, 2011, pp. 1-5.

[10] A. O. Martinez, E. D. Carvalho, and J. O. Nielsen, "Towards very large aperture massive MIMO: a measurement based study," in *2014 IEEE* Globecom *Workshops (GC Wkshps)*, 2014, pp. 281-286.

[11] A. O. Martinez, E. D. Carvalho, J. O. Nielsen, and L. S. Jing, "Frequency dependence of measured massive MIMO channel properties," in *2016 IEEE 83rd Vehicular Technology Conference (VTC Spring)*, 2016, pp. 1-5.

[12] H. Yu, J. H. Zhang, Q. F. Zheng, Z. Zheng, L. Tian, and Y. Wu, "The rationality analysis of massive MIMO virtual measurement at 3.5 GHz," in *2016 IEEE/CIC International Conference on Communications in China (ICCC Workshops)*, 2016 , pp. 1-5.

[13] Q. H. Spencer, A. L. Swindlehurst, and M. Haardt, "Zero-forcing methods for downlink spatial multiplexing in multiuser MIMO channels," *IEEE Transactions on Signal Processing*, vol. 52, no. 2, pp. 461–471, Feb. 2004.

[14] G. Y. Liu, X. Y. Hou, J. Jin, F. Wang, Q. X. Wang, Y. Hao, Y. H. Huang, X. Y. Wang, X. Xiao, and A. L. Deng, "3-D-MIMO with massive antennas paves the way to 5G enhanced mobile broadband: From system design to field trials," *IEEE Journal on Selected Areas in Communications*, vol. 35, no. 6, pp. 1222–1233, Jun. 2017.

[15] A. Paulraj, R. Nabar, and D. Gore, *Introduction to Space-Time Wireless Communications*, Cambridge University Press, 2006.